Available online at www.sciencedirect.com
SCIENCE DIRECT®
International Journal of Mass Spectrometry 243 (2005) 85–93
International Journal of Mass Spectrometry
www.elsevier.com/locate/ijms

Secondary ion emission from CO_2–H_2O ice irradiated by energetic heavy ions Part I. Measurement of the mass spectra

L.S. Farenzena, V.M. Collado, C.R. Ponciano, E.F. da Silveira*, K. Wien[1]

Physics Department, Pontifícia Universidade Católica, Rua Marques de São, Vicente 225, 22543-970 Rio de Janeiro, Brazil

Received 12 August 2004; accepted 30 December 2004
Available online 30 January 2005

Abstract

Secondary ion mass spectrometry is used to investigate ion emission from a frozen-gas mixture ($T = 80$–90 K) of CO_2 and H_2O bombarded by MeV nitrogen ions and by ^{252}Cf fission fragments (FF). The aim of the experiments is to produce organic molecules in the highly excited material around the nuclear track and to detect them in the flux of sputtered particles. Such sputter processes are known to occur at the icy surfaces of planetary or interstellar objects. Time-of-flight (TOF) mass spectrometry is employed to identify the desorbed ions. Mass spectra of positive and negative ions were taken for several molecular H_2O/CO_2 ratios. In special, positive ions induced by MeV nitrogen beam were analyzed for 9 and 18% H_2O concentrations of the CO_2–H_2O ice and negative ions for ∼5% H_2O. The ion peaks are separated to generate exclusive the spectra of CO_2 specific ions, H_2O specific ions and hybrid molecular ions, the latter ones corresponding to ions that contain mostly H and C atoms. In the mass range from 10 to 320 u, the latter exhibits 35 positive and 58 negative ions. The total yield of the positive ions is 0.35 and 0.57 ions/impact, respectively, and of negative ions 0.066 ions/impact. Unexpected effects of secondary ion sputtering yields on H_2O/CO_2 ratio are attributed to the influence of water molecules concentration on the ionization process.

Keywords: Secondary ions; Condensed gases; CO_2–H_2O ice; Electronic sputtering; TOF SIMS; Cluster desorption

1. Introduction

This article is addressed to the question of whether organic material present in the atmosphere or on the surface of the three outer Jovian moons could have partially evolved from heavy ion bombardment of carbon compounds mixed with water ice, the dominant surface material of these moons. The impetus for our work came from an article of Johnson [1], reviewing what is known about the surface conditions of the moons of the planet Jupiter, about the Jovian radiation environment and about surface chemistry induced by the corresponding radiation.

The moons are intensively bombarded by energetic ions and by electrons trapped in the giant magnetosphere of Jupiter. In the case of Europa, the flux of incoming projectiles consists predominantly of hydrogen, oxygen and sulphur ions. At 1 MeV, about 400 oxygen and sulphur ions/(s keV) penetrate the surface per cm^2. There are several indications that carbon-containing compounds exist on the icy surfaces [2–5]. Radiolysis of carbonates could be one source for CO_2, a gas that has been discovered trapped in the icy surfaces of Europa and Callisto [4]. Callisto has a very tenuous atmosphere of CO_2 [4], which does not, however, condense efficiently at its surface temperatures, indicating that the origin of the carbon contained in carbonates and the CO_2 is probably internal. Although the neutrals are principally observed, mass spectrometers have been designed for the proposed Jupiter Icy Moon Orbiter mission to directly detect the ejected ions in order to study surface composition.

* Corresponding author. Tel.: +55 213114 1272; fax: +55 213114 1040.
E-mail address: enio@vdg.fis.puc-rio.br (E.F. da Silveira).
[1] Guest of the Institute of Nuclear Physics, Technical University, 64289 Darmstadt, Germany.

1387-3806/$ – see front matter © 2005 Elsevier B.V. All rights reserved.
doi:10.1016/j.ijms.2004.12.034

The present work is focused on mixtures of frozen carbon dioxide and water, CO_2–H_2O ice and may give values to estimate the sensitivity of a time-of-flight (TOF) detection system designed to operate on Jupiter moons. The method used to identify and characterize the ionic species produced in the surface layers of CO_2–H_2O ice is time-of-flight secondary ion ($SI^{\pm}$) mass spectroscopy, TOF SIMS [6], which has been used to analyze other frozen-gas targets (e.g., [7–9]). The ice was irradiated by MeV nitrogen ions, which eject from the ice surface the produced atomic and molecular ionic species into vacuum. In the energy regime considered, the yield (particles/impact) of neutral particles is generally 2–4 orders of magnitude higher than the yield of charged particles. Mixtures of CO_2 and H_2O gas were condensed on a metallic foil at a temperature of liquid nitrogen.

At the surface temperatures (80–130 K) of the three outer Jovian moons, the CO_2 content of the surface ice layer would decrease steadily by sublimation.

In fact, above a surface temperature of 115 K sublimation hinders the formation of a CO_2 condensate. Therefore, our experiments were performed at the lowest possible target temperatures, i.e., 80–90 K. The concentration of carbon compounds in the uppermost ice layers of the Jovian moons is supposedly small, smaller than a few percent. It turns out that, at such a low CO_2 content, carbon-containing molecular ions are hardly visible in the mass spectra. The issue was to determine the functional dependence of ion yields on the CO_2 concentration in order to extrapolate the yields down to small CO_2 concentrations.

Since the Jovian moons are mainly bombarded by H, O and S ions with up to MeV energies, we used N ion projectiles with energies between 0.4 and 1.7 MeV in measurements and, for comparison, also ∼65 MeV fission fragments. Essential for the secondary ion yield is the energy deposited into the electronic system of the irradiated material, i.e., the electronic energy loss $(dE/dx)_e$ in water, which is for 1.7 MeV N ions 4% smaller than for 1.7 MeV O ions [10]. Since the fluency of the primary ion beam was below $10^7/cm^2$, the chance to detect products of former impact events was negligible. The detected secondary ions are in general ejected from a volume along the nuclear track, whose diameter is 1 or 2 orders of magnitude shorter than the range of the primary ions. Therefore, secondary ion species, which contain beam particles, cannot appear in the TOF mass spectra.

A survey of the chemistry in CO_2–H_2O ice induced by magnetospheric plasma ion bombardment has been recently displayed and discussed by Delitsky and Lane [11]. They list about a dozen different species, which already have been partially found by laboratory experiments using H- and He-beams for irradiation and infrared spectroscopy or quadrupole mass spectroscopy for detection. The emission of these molecules as ions is investigated in the present work.

Secondary ion emission from pure H_2O ice, based on transmission sputtering, has been analyzed recently [12]. For the current work, measurements were also performed with a new method based on backward sputtering, developed to improve mass resolution and to work at constant sputter energy. The work will be presented in two articles: “Measurement of the Mass Spectra” (part I) and “Analysis—Search for Organic Ions” (part II). The first part is presented in this article, where the experimental procedures and findings on positive and negative secondary ions are displayed and partially discussed. The chemical designation of the observed ions and a discussion of ion generation directly formed or due to chemical reactions are treated in part II [13].

2. Experimental methods

The CO_2–H_2O ice samples were irradiated by a 1.7 MeV N^{2+} beam of the Van de Graaff accelerator at the Catholic University of Rio de Janeiro (PUC-Rio) and also by fission fragments of a ^{252}Cf source. Mass spectra of the secondary ions emitted from the ice surface were measured by TOF SIMS [6]. The positive and negative secondary ions $SI^{\pm}$ were produced by two different sputter modes: forward sputtering and backward sputtering. Common to both modes is the fact that the energy loss of the N ions in the target was used to determine the thickness of the ice layer being deposited by continuous condensation on the target carrier, a thin metal foil. Measurement of the ice layer thickness occurred simultaneously with acquisition of the mass spectra and allowed the determination of the momentary growth rate of the ice layer.

2.1. First method: forward sputtering

In the forward (or transmission) sputtering method, the 1.7 MeV N^{2+} beam of the accelerator impinges on the back of the target at an angle of 45°. It traverses first the target substrate, a thin Al foil, and then the ice layer condensed from a steady flow of the CO_2–H_2O gas. The secondary ions of interest are those ejected from the front of the target.

The TOF technique is employed to determine both the mass spectra of the secondary ions and the ice layer thickness [12].

Forward sputtering was used to measure the functional dependence of $SI^{\pm}$ yields on the concentration of CO_2 in the CO_2–H_2O gas mixture. A disadvantage of the method is that, during continuous condensation, the widths of mass lines increase during data acquisition (as the ice thickness increases, both the projectile energy straggling also increases and the start signal delays) and weak mass lines became unresolvable. Furthermore, it was difficult to reproduce the same ice layer thickness by condensation of a new CO_2–H_2O gas mixture: the target exit energy, the sputter energy, was not constant and difficult to monitor.

2.2. Second method: backward sputtering

The corresponding experimental setup is sketched in Fig. 1. In this arrangement, the projectile ions penetrate the ice layer at the target front side, from where the $SI^{\pm}$ are

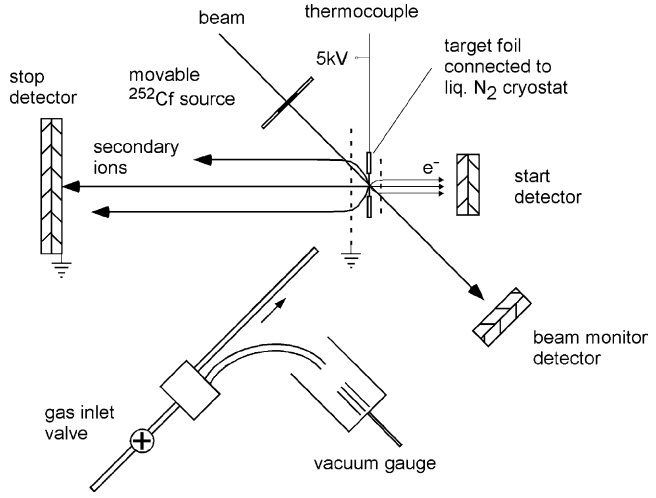

Fig. 1. Experimental setup used to produce secondary ions from frozen gases by means of the backward sputtering method. Irradiation could be alternatively produced by the accelerator beam or by fission fragments from a ^{252}Cf source.

backward ejected with respect to the incident beam and accelerated towards the stop detector being equipped with two microchannel plates. Secondary electrons produced by the projectile ions at the target backside are accelerated to about 2 keV and then detected by a second channel plate assembly for generating start signals. These start signals have a very accurate timing, independent of the ice layer thickness. The range of mass resolution is $m/\Delta m = 850$–1200 at $m = 100$ u, limited essentially by the initial energy distribution of the $SI^{\pm}$. After exiting the target, the projectile ions travel a distance of 22.8 cm and impact a third channel plate detector, which is used to monitor the beam intensity and to measure by TOF the energy of each detected beam ion. The energy difference to the original beam energy is used to calculate, by means of energy-loss tables [10], the momentary ice layer thickness (see also next section).

The monitor detector was also used to measure absolute ion yields by setting a coincidence condition on the start signals. The TOF spectrum is measured then only for those beam ions, which had passed the target and were definitively detected and counted. Due to angular scattering in thick targets, the number of ions being detected in the monitor counter was often much smaller than the number of start detector signals. Therefore, some mass spectra were recorded without and with coincidence condition, in order to obtain relative ion yields with good statistics (statistical error ±10% for a yield of 0.001 ions/impact in Fig. 5a) and absolute yields sufficiently accurate only for the high peak ions. The main error of absolute yields is attributed to the detection efficiency for the ejected ions (0.5 ± 0.1, including grid transmission). Regarding absolute yields, the systematic errors add up to ±25%.

A thermocouple is directly connected to the Cu plate that holds the target foil and used to apply an acceleration voltage of ±5 kV to the target. As seen in Fig. 1, the gas flow, from which the ice layer is condensed, is split twice: one flow is directed to the target, while the second one goes to a separated vacuum gauge. This method allows stabilizing the gas pressure in front of the target in the range from 2×10^{-7} mbar up to 1.5×10^{-4} mbar. The accelerator beam can be replaced by fission fragments emitted from a movable ^{252}Cf source. The energy of the fission fragments behind a cover foil is about 65 MeV.

2.3. Preparation of the ice layer

Two series of TOF mass spectrometry experiments were performed using the two types of sputtering modes but also two different methods of target preparation: The ice targets were condensed first from CO_2 gas and H_2O gas mixed in a mixing chamber [12] and second from pure CO_2 gas (99.998%) and the H_2O gas contained in the rest gas of the vacuum chamber. The latter method was set up from the observation that, at the basic pressure of about 2×10^{-7} mbar, contamination of the ice sample by rest gas was unavoidable and falsified the relative concentrations of the CO_2–H_2O ice. The rest gas consisted mainly of H_2O gas (>85%). Fig. 2 shows a typical TOF mass spectrum of a rest gas condensate. The $(H_2O)_nH_3O^+$ cluster series (see Ref. [12]), which carries for pure H_2O ice 70% of the H_2O specific ion yield, dominates the spectrum. Typical signals of the organic rest gas component are the hydrocarbon ions $C_nH_m^+$ at masses 27, 29, 39, 41, 43, 53, 55, 57, 59, 61 u, etc., all odd mass ions. The organic rest gas component stems mainly from pump oil.

When the mixing was performed in a separate stainless steel chamber, the relative concentration of the two gases CO_2 and H_2O was adjusted by means of their partial pressures (total pressure about 5×10^{-2} mbar). In order to reduce contamination of the ice target by rest gas condensation, the ice layer was continuously refreshed by directing a weak, steady flow of the gas onto the cold target. The content of rest gas H_2O in the ice layer remained nevertheless considerable high (>5%): the rest gas condensation modified the actual CO_2 concentration of the ice sample, so that this was always smaller than that of the gas mixture before condensation

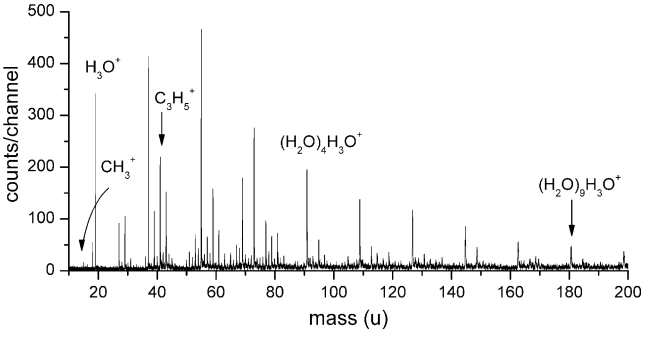

Fig. 2. TOF mass spectrum of the rest gas condensed at $T = 80$ K. The spectrum was measured at a basic pressure of 2×10^{-7} mbar with a growth rate of 0.075 μg/(cm^2 min). The ice layer thickness corresponds to 95 monolayers of H_2O. Irradiation was performed with 1.7 MeV N^{2+} ions during 100 s.

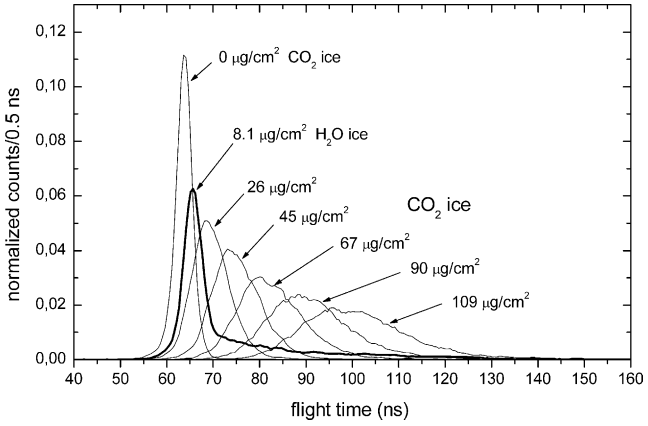

Fig. 3. TOF distributions of the nitrogen beam ions after passing the target covered by an ice layer, whose thickness was growing from 0 to 109 μg/cm^2. For clarity, only eight time distributions, out of the 16 measured ones, are shown. The distributions are normalized to the integral number of counts per distribution.

(see Section 3.3). This was particularly true for high CO_2 concentrations; the minimum H_2O concentration achievable was about 5%. Therefore, the background of organic mass lines seen in Fig. 2 was unavoidable.

A method was set up to reduce this background by increasing the rate of pure CO_2 condensation relative to that of rest gas condensation. For this, the CO_2 pressure in front of the target was increased up to about 10^{-4} mbar. The resulting H_2O concentration of the ice layer was then determined by means of the CO_2 growth rate and the rest gas-growth rate as described by the following procedure:

- sixteen mass spectra and 16 flight-time distributions of the projectile ions after they have traversed the target are simultaneously taken during steady ice layer growth (see Fig. 3);
- the mean time values of each distribution are used to calculate the corresponding mean energy loss;
- the CO_2 ice layer thickness is determined by entering this energy loss into the energy-loss table [10]. Fig. 4 illustrates the function d(t), which relates the thickness d on time t;
- the momentary growth rate $\Delta d/\Delta t$ in μg/(cm^2 min) is determined through the derivative of the function d(t) of the ice layer;
- shortly before the start of the measurement of the last (the 16th) time distribution, the target temperature is quickly increased and the last measurement started. During this measurement, the layer thickness decreases, the flight times become shorter, and the time distributions move quickly to smaller flight times. This generates the thick line shown in Fig. 3, which ends up in a relatively narrow distribution, indicating that – in the second half of the time period – all CO_2 ice disappears from the target and that the layer left has a thickness equivalent to 8.1 μg/cm^2 H_2O ice (at about 120 K);
- such residual ice layers are used to determine the mean growth rate of the rest gas condensation and to estimate then the H_2O concentration of the ice samples being condensed from pure CO_2 gas and the H_2O contained in the rest gas.

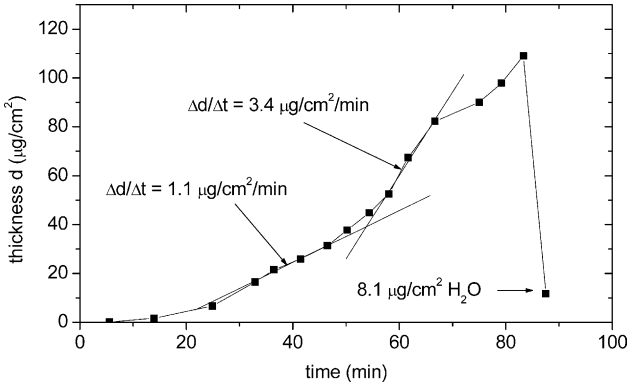

Fig. 4. Thickness, d, of the CO_2–H_2O ice layer as a function of the time, t, of condensation. For two portions of the curve $d(t)$, the momentary growth rate has been evaluated. These two rates correspond to two different CO_2 pressures in front of the target. The presented curve is derived from the TOF distributions shown in Fig. 3.

Since irradiation and condensation of the ice occur simultaneously, the structure of the uppermost ice layers has to be considered as amorphous at the moment of ion impact. Above 130 K, amorphous H_2O ice turns into crystalline phase, but tends to crystallize also below 130 K as time goes by, as revealed in detail by Kouchi and Yamamoto [14]. Due to the relatively very long time scales, the ice grains on the surfaces of the Jovian moons should be crystalline although the irradiated surface layers might be amorphous.

3. Experimental results and discussion

Two methods have been employed to measure the TOF mass spectra: (i) the forward sputtering mode, making use of a mixing pre-chamber and (ii) the backward sputtering mode and mixing pure CO_2 directly with H_2O contained in the rest gas. For both series of experiments, the targets were irradiated by 1.7 MeV N^{2+} ions having a current of 1000–2000 ions/s on the target (diameter: 5 mm). The target temperature was kept at 80–90 K. The resulting high-resolution mass spectra of the second series of experiments will be presented first.

3.1. Mass spectra obtained by the backward sputtering method

Mass spectra of positive and negative secondary ions are presented in Figs. 5 and 6, respectively.

3.1.1. Positive ions

Two positive ion spectra are selected for detailed analysis: one measured with a growth rate of 5.6 μg/(cm^2 min), and another one with 3.1 μg/(cm^2 min). In both cases, after evaporation of the CO_2, the thickness of the remaining rest gas condensate was determined and used to evaluate the H_2O

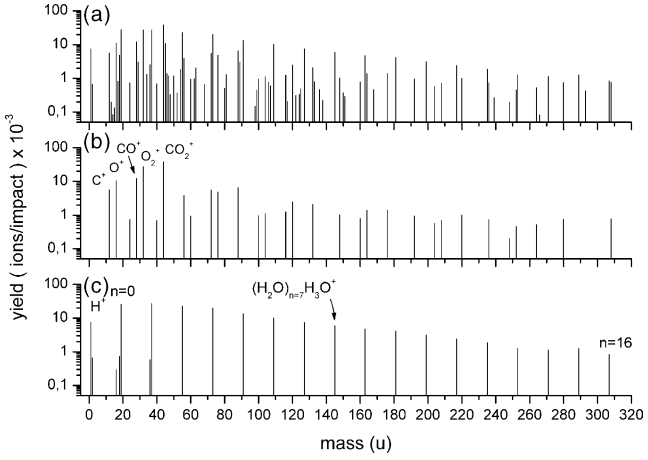

Fig. 5. Positive ion mass spectrum of: (a) CO_2–H_2O ice target, with 9% H_2O concentration (the background spectrum has been subtracted), (b) CO_2 specific ions (as it appears in the total spectrum) and (c) H_2O specific ions. The relative intensities of the weak mass lines O^+, H_2O^+ and $(H_2O)_2^+$ were taken from pure H_2O ice spectra [12].

growth rate, 0.36 and 0.35 μg/(cm^2 min), respectively. The resulting H_2O concentrations were (9 ± 2)% and (18 ± 3)% (molecules%). In order to identify the background mass lines, these two mass spectra taken with different growth rates were compared: the spectrum measured with 18% H_2O ice exhibits a $(H_2O)_nH_3O^+$ series, whose relative intensity was 3.5 times higher than that obtained with 9% H_2O ice. Accordingly, the relative intensity of background lines is considerably higher in the first spectrum. In the mass range between 26 and 81 u, we were able to identify 20 mass lines, which were mainly composed from background events.

In order to eliminate the background, the condensed rest gas spectrum shown in Fig. 2 was employed to provide the relative yields of the background lines. After normalization, the background lines were subtracted. The resulting spectrum measured with 9% H_2O ice is shown in Fig. 5a. The relative yield of the original background was 6% of the total positive ion yield. Some lines at background positions remained. When they had a yield below a certain limit – depending on the ion intensities in the rest gas spectrum – they were disregarded. Thus, it is possible to assign for such ions only a lower yield limit Y_{lim}. For an ion of mass 43 u – this mass corresponds to the highest line of the background – this limit is $Y_{lim} = 0.0024$ ions/impact. For an ion of mass 13 u, no background mass line was observed, $Y_{lim} = 0.00003$ ions/impact. The later limit was derived from the events between the mass lines, which are mainly generated by chance coincidence events. The H_2O specific mass lines in the spectrum of Fig. 5a have their original intensity.

The same procedure for eliminating the background is used to elaborate the mass spectrum of the CO_2–H_2O ice measured with an H_2O content of 18%. The resulting spectrum is similar to that shown in Fig. 5a. As seen in Table 1, the total yields of the positive ions are higher than those for the 9% H_2O concentration. It is observed that the positive ion yield for N^{2+} beam (9% H_2O ice) is mainly composed by H_2O specific ions (50% of the total), against 39% of CO_2 specific ions and 11% of hybrids.

3.1.2. Negative ions

A similar procedure was employed to eliminate the very low background (0.3% of the negative ion yield) in the negative ion spectrum. Because the CO_2 growth rate (7.1 μg/(cm^2 min)) was higher than in case of the experiments for positive ions, the H_2O concentration was only about 5%. Fig. 6a shows the negative ion spectrum measured with 5% H_2O concentration.

In Fig. 5b and c as well as in Fig. 6b and c, mass spectra are generated with selected lines of the CO_2 and H_2O specific ions, taken with the same yields from the total spectra in Fig. 5a and Fig. 6a, respectively. A summary of the measured desorption yields is also given in Table 1. Contrary to the positive secondary ions, the negative ion yield (for ∼5% H_2O) is mainly due to CO_2 specific ions (77%), against 7% of H_2O specific ions and 16% of hybrids.

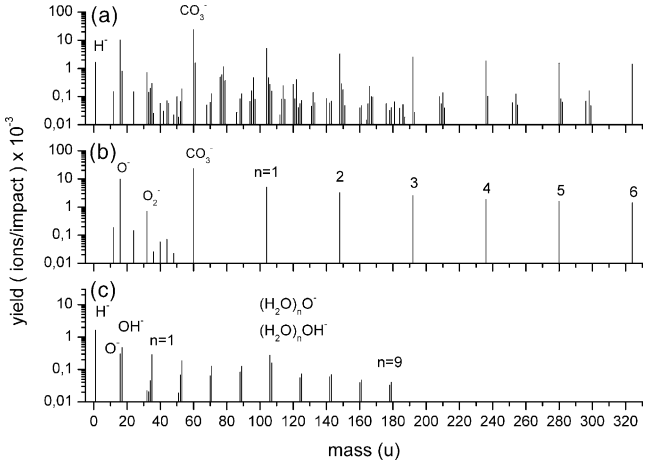

Fig. 6. Bar spectrum of (a) negative secondary ions ejected from CO_2–H_2O ice with 5% H_2O concentration. The background spectrum was subtracted; (b) CO_2 specific ions as it appear in the total spectrum (a); (c) H_2O specific ions having again the same yields as in the total spectrum. The relative intensities of the mass lines at $m = 33$ and 34 u were taken from pure H_2O ice spectra [12].

Table 1
Yields of secondary ions ejected from CO_2–H_2O ice by 1.7 MeV N^{2+} ions

	Yield ions/impact ($\times 10^{-3}$)		
	Positive ions	Positive ions	Negative ions
H_2O concentration	9%	18%	∼5%
Total ion yield	349	574	66
CO_2 specific ions	134	112	51
H_2O specific ions	174	414	4.4
Hybrid molecular ions	41	48	10.1

The H_2O concentration was 9, 18 and ∼5%, the target temperature about 90 K. Yields of background ions are not taken into account.

Table 2
Yields of CO_2 specific ions

	Yield ions/impact ($\times 10^{-3}$)			
	1.7 MeV N^{2+}	1.7 MeV N^{2+}	0.66 MeV $N^{(eq)}$	$FF^{(eq)}$
H_2O concentration	9%	18%	≅10%	≤10%
C^+	5.7	3.6	1.9	305
$(CO_2)C^+$	3.9	5.7	0.54	39
O^+	11	4.7	3.0	302
$(CO_2)_{n=1-4}O^+$	4.1	6.5	1.1	37
O_2^+	28	17	6.1	626
$(CO_2)_{n=1-3}O_2^+$	8.8	13	1.6	86
CO^+	12	8.1	3.4	492
$(CO_2)_{n=1-4}CO^+$	8.2	19	1.1	59
CO_2^+	39	24	8.2	575
$(CO_2)_{n=1-6}CO_2^+$	13	10.7	1.1	100
	1.7 MeV N^{2+}		0.86 MeV $N^{(eq)}$	$FF^{(eq)}$
H_2O concentration	∼5%		≅10%	≤10%
C^-	0.16		0.2	10
O^-	10.0		3.5	234
O_2^-	0.71		0.22	184
CO_2^-	0.06			1.8
C_2O^-	0.07			1.8
$C_{n=2-4}^-$	0.20		0.15 (C_2^-)	7.3 (C_2^-)
CO_3^-	24.1 (19.2)[a]		4.9	460
$(CO_2)_{n=1-6}CO_3^-$	16.0 (11.8)[a]		1.7	220

The yields of cluster ions belonging to one series have been summed over n, the number of cluster constituents. The range of n considered is the same for all columns.

[a] The yields in brackets are the yields of promptly ($<10^{-10}$ s) ejected ions. The yields before the brackets include delayed emission (see Ref. [13]). (eq) means charge-equilibrated projectiles.

3.2. CO_2 specific ions

Positive secondary ion mass spectra of pure CO_2 ice being irradiated by 1.5 MeV/u Ar^{4+} ions were published by Tawara and coworkers [15]. They found as main products the cluster series $(CO_2)_nR^+$, with the radical $R^+ = C^+$, O^+, CO^+, O_2^+ and CO_2^+, and weaker contributions of C_2^+ and C_3^+. All these positive ions have been observed in the present spectra (Fig. 5b) and their yields are listed in Table 2. So far, a mass spectrum of the negative CO_2 specific ions has not been published. The negative ion spectrum shown in Fig. 6b is dominated by a mass line at $m = 60$ u, the CO_3^- ion, and by the corresponding cluster series $(CO_2)_nCO_3^-$.

Comparing the total yields of CO_2 specific ions measured with projectile energies of 0.66, 1.7 and 65 MeV and similar H_2O concentrations (see Table 2), they scale on an average with the electronic energy loss, when a threshold energy loss of $(dE/dx)_{thres} = 31$ eV/Å is taken into account:

$$Y_{CO_2} = Y_0^{\pm}\left(\frac{dE}{dx} - 31\,\mathrm{eV/\AA}\right)$$

with $Y_0^+ = 0.0047$ ions/(impact eV/Å) for positive ions and $Y_0^- = 0.0020$ ions/(impact eV/Å) for negative ions. This linearity is in fair agreement with primary ionisation along the nuclear track which is roughly linear in $(dE/dx)_e$, the electronic energy loss [16,17]. The total sputter yield scales better with the second power of $(dE/dx)_e$ [16,18]. Note that the H_2O/CO_2 fraction in the ice plays a special role in the emission yield of CO_2 specific ions (fragments and reaction products). For 1.7 MeV N irradiation, going from 9% H_2O to 18% H_2O ice, the yields of the radical ions R^+ (C^+, O^+, CO^+, O_2^+, CO_2^+) decrease by a factor of about 0.6 while the ionic reaction products $(CO_2)_nR^+$ (except $(CO_2)_nCO_2^+$) increase by a factor of 1.6. For further discussion of CO_2 specific ions, see part II of this work [13].

3.3. H_2O specific ions

The chemical designation of the H_2O specific ions is known from literature ([12] and references therein). Both, the positive and the negative ion spectra exhibit cluster series: their yields listed in Table 3 are the same as observed in the total spectra (Fig. 5a and Fig. 6a). Exceptions are the yields of the ions O^+, H_2O^+ and $(H_2O)_2^+$ as well as O_2^-, $(H_2O)O^-$ and $(H_2O)OH^-$. They are lower than the reported yields taken from spectra obtained with pure H_2O ice [12]. The actual intensities of these ions are increased due to the presence of CO_2 in the ice. The opposite effect is observed for H^+ and H_2^+: the relative yields of the two ions are much higher for pure H_2O ice than for mixed ice.

Results on H_2O specific ions, in particular the $(H_2O)_nH_3O^+$ cluster series, have been already discussed in Ref. [12]. The total mass spectrum measured with only 9% H_2O concentration is still dominated by the $(H_2O)_nH_3O^+$ series. This is an effect of preferential proton incorporation in water molecules. From 18 to 9% H_2O concentration,

Table 3
Yields of H_2O specific ions, ejected from CO_2–H_2O ice bombarded by 1.7 MeV N^{2+} ions

H_2O concentration	Yield ions/impact ($\times 10^{-3}$)		
	9%	18%	~5%
H^+, H_2^+	7.5, 0.67	48, 5.0	
H_3O^+	28	43	
$(H_2O)_n{\cdot}H_3O^+$ (n = 1–6)	129	267	
$(H_2O)^+$, $(H_2O)_2^+$, $(H_2O)_3^+$	4.9, 2.6, 1.5	26, 12, 13	
H^-			1.65
O^-			0.31
OH^-			0.48
$(H_2O)_nO^-$ (n = 1–9)			0.73
$(H_2O)_nOH^-$ (n = 1–9)			1.14

the yield of this cluster series (n = 1–16) decreases by a factor of 2.1. The designation $(H_2O)_nH_3O^+$ was chosen because it has been assumed that the water clusters are associated with hydronium ion surrounded by water molecules and not H^+ attached to the clusters [19–21]. However the species $H_5O_2^+$, surrounded by water molecules, cannot be excluded as the ionic unit [21]. It was also found that for CO_2–H_2O ice the yields of the cluster ions decrease with n faster than for pure H_2O ice. For 9% H_2O concentration, the mean value of n is 4.2, while for pure H_2O ice it is 5.5.

3.4. Hybrid molecular ions

After subtracting the spectra displayed in Fig. 5b and c, and Fig. 6b and c from the total spectra in Fig. 5a and Fig. 6a, mass lines of ions remain, which are called now on "hybrid molecular ions". They are attributed to reactions between CO_2 specific atoms, molecules and ions and H_2O specific atoms, molecules and ions. Most of these hybrid molecular ions contain C and H atoms. OH^+, for instance, could have been produced by H_2O specific species only, but it is seldom or never found in mass spectra obtained with pure H_2O ice [12]. In the mass range up to 325 u, 35 positive hybrid molecular ions were identified and 58 negative ones. Their total yields are given in Table 1.

The analysis of the hybrid molecular ions is one of the main subjects of part II of this work [13].

3.5. Measurements using ^{252}Cf fission fragments for irradiation

The spectra obtained with the 1.7 MeV N^{2+} ion beam are compared with spectra measured with ^{252}Cf fission fragments (FF) by means of the first method (see Section 2.1 and Ref. [12]). One FF impacts the ice target at the front side and the complementary fission fragment is used to generate the start signal. The corresponding mass resolution is about 170 at m = 100 u. TOF mass spectra obtained with CO_2–H_2O ice having about 50 and 10% H_2O concentrations are shown in Figs. 7 and 8. In these measurements, growth rates were not measured with FF. Background caused by rest

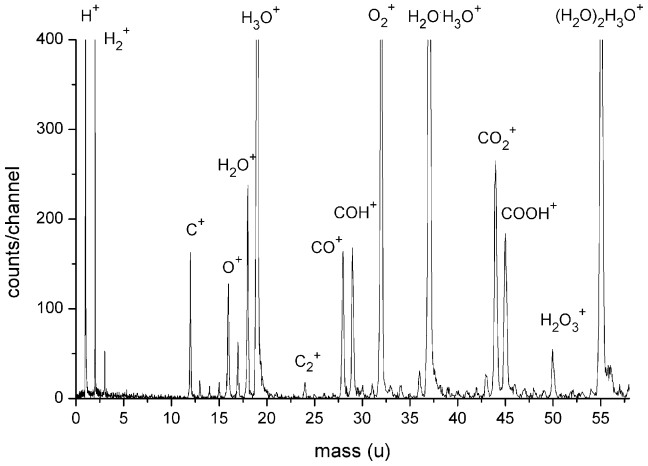

Fig. 7. Section of the positive mass spectrum of CO_2–H_2O ice, irradiated by fission fragments during 600 s. The concentrations of CO_2 and H_2O were about 50%. The chemical designation of various mass lines like COH^+ and $COOH^+$ is explained in Ref. [13]. The background was not subtracted.

gas contamination is indicated by many low intensity mass lines as, for instance, seen in Fig. 7 between m = 30 and 54 u.

All the identified CO_2 specific ions are listed in Table 2. The variety of detected hybrid molecular ions obtained with FF is smaller: in the positive ion spectrum (Fig. 7) the peaks corresponding to the ions OH^+, COH^+, $COOH^+$ and to the cluster series $(CO_2)_nH^+$ and $(H_2O)_n(CO_2)H_3O^+$ are clearly observed. Their chemical assignment and the formation of the very weak peaks due to the CH^+, CH_2^+ and CH_3^+ ions will be discussed in part II of this work [13]. Despite the low H_2O concentration ($\leq$10%) used to measure the negative ion spectrum seen in Fig. 8, negative hybrid molecular ions show up with relatively high intensity above the CO_3^- ion at m = 60 u. Most prominent are the $(CO_4H_{m=0-3})^-$ group and

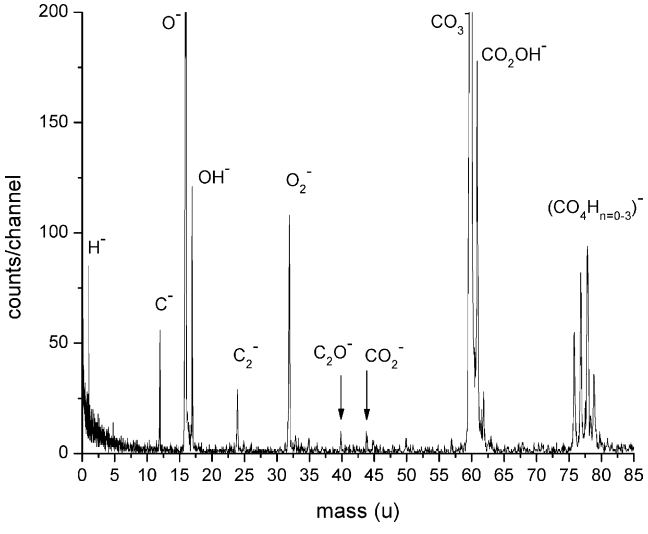

Fig. 8. Section of the negative mass spectrum of CO_2–H_2O ice, irradiated by fission fragments during 600 s. The concentration of H_2O was about 10%. The chemical designation of various mass lines like those of the $(CO_4H_{m=0-3})^-$ group is explained in Ref. [13]. The background was not subtracted.

corresponding cluster ions. The yields presented in Table 2 for fission fragment irradiation were obtained with ice having the lowest H_2O concentration achievable.

3.6. Measurements as function of CO_2 concentration

In order to prepare ice layers of CO_2–H_2O mixtures, these gases were mixed in a separate stainless steel container by means of their partial pressures. A needle valve was used to direct a steady, very weak flow of gas onto the cold target, where it condensed. In order to obtain clean mass spectra, each TOF spectrum measurement was performed with a freshly prepared gas mixture, i.e., the mixing pre-chamber was emptied and then refilled with fresh gases. Using the first method, the transmission sputtering, several mass spectra were measured with different CO_2 concentrations. For the CO_2 specific ions, the main result of this experiment is that the yields of the most intensive CO_2 specific ion peaks (see Table 2) increase—between 30 and 80% CO_2 content—exponentially with CO_2 concentration. It is important to remark that the yield of H_2O specific ions, for instance that of the $(H_2O)_nH_3O^+$ series, did not vanished when pure CO_2 was introduced in the mixing chamber. This means that the condensation of the residual gas in the main chamber was modifying the expected CO_2 concentration of the condensed ice. The results presented here (see Table 2) correspond to CO_2 specific ions measured with the lowest possible H_2O concentration (≅10%) and with N ions having exit energies of 0.66 and 0.86 MeV (the equilibrium charge states are 2.3 and 2.5, respectively).

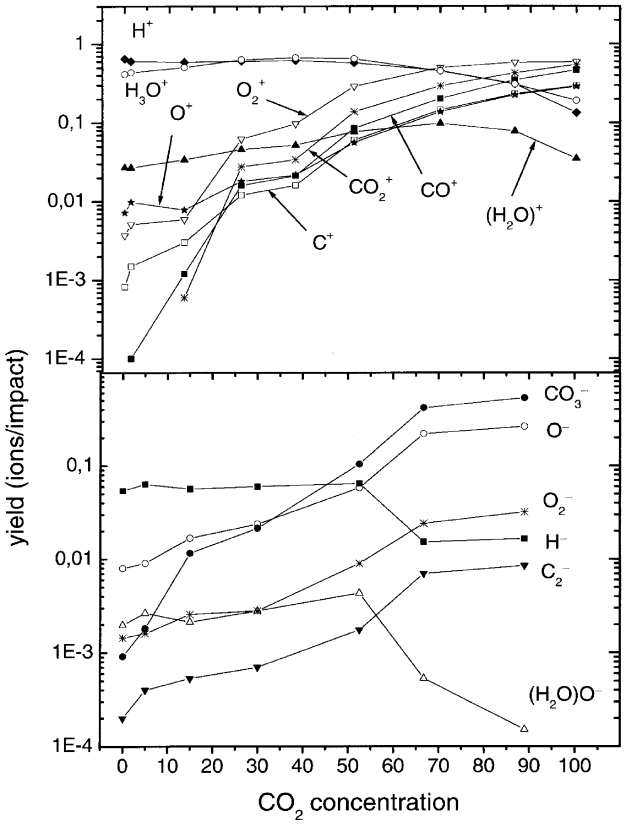

Fig. 9. Yields of (a) positive and (b) negative secondary ions measured as a function of the CO_2 concentration in the mixing chamber. The ice targets were irradiated by fission fragments.

Very instructive are the yield curves measured with FF impacting on ices condensed from various CO_2–H_2O gas mixtures in the mixing chamber. Again, the CO_2 concentration of the ice layer is not very precise due to the water vapour in the main chamber residual gas, but certain trends are observable. In Fig. 9, yields of positive CO_2 and H_2O specific ions are plotted versus the CO_2 concentration of the gas in the mixing chamber. The curves of H_2O specific ions like H^+, H_3O^+, H_2O^+ and the cluster ions $(H_2O)_nH_3O^+$ are supposed to decline to zero at 100% CO_2, but—as mentioned—the actual CO_2 content of the ice in the main chamber is somewhat lower than that in the mixing chamber. The yield curves of the ions C^+, CO^+ and $CO_2{}^+$ are quite similar, they increase exponentially between 25 and 70% CO_2 concentrations.

4. Summary

The secondary ion mass spectrometry (TOF SIMS), in which MeV ions are used to induce electronic excitations inside frozen-gas samples, shows to be a very sensitive method to probe the formation and emission of hybrid ions, as well as to study the distribution of the ionic cluster abundance as a function of the sample composition. The findings of the present work are particularly applicable to the astrophysical subject of sputtering of cometary and planetary surfaces.

The sputtering of the CO_2–H_2O ice was studied for different molecular ratios. The absolute positive and negative ionic sputtering yields were determined and show expected (e.g., as the ratio CO_2/H_2O increases, the CO_2 yields increase) and unexpected behaviors, as for instance: (a) the H_3O^+ cluster yield increases, has a maximum around 40% mixture and then decreases; (b) the $(H_2O)O^-$ yield increases slowly till 50% mixture and then drops strongly. These unexpected effects are probably due to the influence of water molecules concentration on the ionization process.

The used method detects particularly the ions formed within 10^{-10} s after the projectiles impact. It is difficult to draw conclusions from the yield of a certain molecular ion based on the total yield of this molecule; the neutral molecular yield can be 2–4 orders of magnitude higher than the ion yield. A rough estimate leads to 5×10^{-6} to 5×10^{-4} hybrid molecular ions per impact in the flux of sputtered particles at a CO_2/H_2O ratio of about 1/1. In spite of the fact that the secondary ions correspond to a very small fraction of the total sputtered flux, they probably reveal the whole spectrum of compounds, ejected either from the icy surface or from the ice bulk, the latter being produced inside the nuclear track plasma within 10^{-10} s after the projectiles impact. These compounds react further with the CO_2–H_2O ice matrix or among themselves. TOF SIMS can be also used to detect

such late products as well as the prompt (stable) products. Taking into account the absolute yields measured here, a flux of 5×10^{15} to 5×10^{17} 1.7 MeV N ions/cm^2 is required to convert 1% of the irradiated material into hybrid molecular ions.

References

[1] R.E. Johnson, Energetic Charged Particles Interactions with Atmospheres and Surfaces, Springer-Verlag, Heidelberg, 1990.
[2] T.B. McCord, et al., J. Geophys. Res. 104 (1999) 11827.
[3] R.W. McCord, et al., Science 280 (1998) 1242.
[4] R.W. Carlson, Science 283 (1999) 820.
[5] J.M. Moore, et al., Icarus 140 (1999) 294.
[6] K. Wien, Nucl. Instr. Meth. B 131 (1997) 38.
[7] E.F. da Silveira, C.D. McAfee, D.L. Cocke, D.G. Naugle, D. Sun, E.A. Schweikert, Int. J. Mass Spectrom. Ion Processes 91 (1989) 5.
[8] R.L. Betts, E.F. da Silveira, E.A. Schweikert, Int. J. Mass Spectrom. 145 (1995) 9.
[9] K. Wien, C.S.C. de Castro, Nucl. Instr. Meth. B 146 (1998) 178.
[10] L.C. Northcliffe, R.F. Schilling, in: K. Way (Ed.), Nuclear Data Tables, vol.7, Nos. 3–4, 1970.
[11] M.L. Delitsky, A.L. Lane, J. Geophys. Res. 102 (E7) (1997) 385.
[12] V.M. Collado, L.S. Farenzena, C.R. Ponciano, E.F. da Silveira, K. Wien, Surf. Sci. 569 (2004) 149.
[13] C.R. Ponciano, L.S. Farenzena, V.M. Collado, E.F. da Silveira, K. Wien, Secondary Ion Emission from CO_2–H_2O Ice Irradiated by High Energetic Heavy Ions. Part II: Analysis—Search for Organic Molecular Ions, Int. J. Mass Spectrom, in press.
[14] A. Kouchi, T. Yamamoto, Prog. Crystal Growth Charact. Mater. 30 (1995) 83.
[15] H. Tawara, T. Tonuma, H. Kumagai, T. Matsuo, H. Shibata, J. Chem. Phys. 94 (4) (1991) 2730.
[16] R.E. Johnson, Chemical Dynamics in Extreme Environments, ed. R.A. Dressler, Advanced Series in Physical Chemistry 11 (2000) 390.
[17] R.L. Fleischer, P.B. Price, R.M. Walker, Nuclear Tracks in Solids Principles and Applications, Berkeley, CA, 1995.
[18] W.L. Brown, W.M. Augustyniak, E. Simmons, K.J. Marcantonio, L.J. Lanzerotti, R.E. Johnson, J.W. Boring, C.T. Reimann, G. Foti, V. Pirronello, Nucl. Instr. Meth. 198 (1982) 1.
[19] R. L. Johnston, Atomic and Molecular Clusters, ed. D.S. Betts, Masters Series in Physics and Astronomy (2002) 64.
[20] S. Wei, Z. Shi, W. Castelman Jr., J. Chem. Phys. 94 (1991) 3268.
[21] T.S. Zwier, Science 304 (2004) 1119 (published online 29 April 2004; 10.1126/science, 1098129).